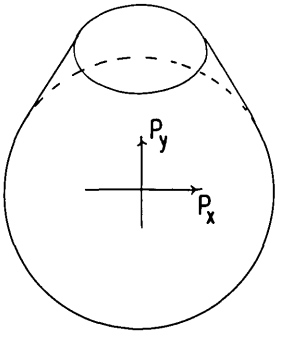

FIG. 6. The solid angle subtended by an infinite truncated cone.

the point of observation moves, but the ellipse moves and changes in size and shape. Clearly the directions of **J** derived from such a source could not coincide with those from the semi-infinite line, since all points along the projection of the line are equally weighted, whereas this is not the case for points along the line of symmetry in Fig. 6.

Thus, the lines of flow of **J** for a truncated cone will not coincide with the usual mirror shapes for a 3D compound parabolic concentrator; this is one reason why this system cannot be ideal, since we know that the parabolic shape is essential to control the meridian rays properly.

Furthermore, we can see that the outline in Fig. 6 does not have a second plane of symmetry at right angles to that shown. This means that, even if we were to determine the lines of flow for the truncated cone, the condition of detailed balance of the rays (Sec. III) at a mirror along the flow lines could not be fulfilled. Thus, the flow at other regions would be perturbed, and the concentrators would not be ideal.

We conclude from this argument that a rotationally symmetric concentrator of compound parabolic concentrator type cannot have maximum theoretical concentration ratio.

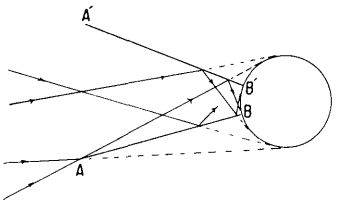

FIG. 7. The light cone as a surface lying in the lines of flow from a sphere.

VI. THE LIGHT CONE

As a final example we show how the light cone can be derived from the lines of flow of the vector flux. We take as starting point a spherical Lambertian radiator, as in Fig. 7. From symmetry, the lines of flow are straight lines passing through the center of the sphere and, also from symmetry, the rays are in detailed balance for any surface element with flow lines lying in it. Thus any conical surface with the center of the sphere as vertex forms an ideal concentrator; however, the source here is virtual and it is bounded by the sphere. Thus the concentrator takes all rays through points in the entry aperture AA' which are aimed at points on the sphere and reflects them to points inside the exit aperture BB'. The right circular cone is a special case among all these possible cones.

ACKNOWLEDGMENT

This research was supported in part by the U.S. Department of Energy, Division of Advanced Energy Projects.

[1]R. Winston and W. T. Welford, J. Opt. Soc. Am. **69**, 532–536(1979) (this issue).
[2]R. Winston, J. Opt. Soc. Am. **60**, 245–247 (1970).
[3]W. T. Welford, and R. Winston, *The Optics of Nonimaging Concentrators* (Academic, New York, 1978).
[4]A. Rabl and R. Winston, Appl. Opt. **15**, 2880–2883 (1976).

Statistical properties of counting distributions for intensity-modulated sources

Paul R. Prucnal and Malvin Carl Teich.
Department of Electrical Engineering and Computer Science, Columbia University, New York, New York 10027
(Received 21 August 1978)

Statistical properties such as the cumulants, and the central, factorial, and ordinary moments are obtained for photocounting distributions when the incident radiation is intensity-modulated with arbitrary statistics. The results are applied in some detail to the cases of triangular, sinusoidal, and square-wave modulation of multimode superposed coherent and chaotic radiation. The coefficient of variation, skewness, and kurtosis are obtained as a function of modulation depth. Comparison is made with experimental data in the cases of triangular and sinusoidal modulation of a laser source.

INTRODUCTION

The great variety of photocounting distributions that can be generated with intensity-modulated radiation is by now well known.[1–15] It is evident that modulation broadens these distributions; this can be interpreted as an accentuation of photon bunching since both low- and high-count probabilities are increased at the expense of counts near the mean. Indeed, the extent of the broadening appears to depend strongly on the intensity distribution of the underlying radiation.[6] However, the counting distributions for intensity-modulated radiation can be characterized by a number of widely recognized and accepted statistical parameters, which have thus far received little attention.

Such modulation is sometimes deliberate, but more often

 0030-3941/79/040539-06$00.50

is unavoidable. It may be imparted to the underlying radiation by mechanisms as diverse as transmission through a stochastic channel (e.g., the turbulent atmosphere[7,9]) and power-supply ripple.[6] It is also important when the source is pulsed (e.g., exponentially decaying[14]) rather than continuous. The analysis presented here applies also to nuclear counting[5] and neural counting.[16] It will generally not be applicable in the presence of dead time.[17]

In this paper detailed statistical properties such as the cumulants, and the central, factorial, and ordinary moments are obtained for counting distributions when the incident radiation is intensity modulated with arbitrary statistics. Our calculations are valid for the case where the integrated intensity is separable into a product of modulation-dependent and modulation-independent components. The results are applied to the cases of triangular, sinusoidal, and square-wave modulation of superposed coherent and chaotic radiation. The coefficient of variation, skewness, and kurtosis are obtained as a function of modulation depth. Comparison is made with experimental data in the cases of triangular and sinusoidal modulation of a laser source.

THEORY

The intensity is assumed to be expressible as the product of two independent, stationary, ergodic random processes

$$I(t) = m(t)I_0(t), \tag{1}$$

where $m(t)$ represents the modulation (with correlation time τ_m) and $I_0(t)$ represents the intensity of the underlying radiation (with coherence time τ_0). The integrated intensity

$$W = \int_t^{t+T} \eta m(t')I_0(t')\,dt' \tag{2}$$

is independent of t for the stationary, ergodic processes considered here. The observation interval is from t to $t + T$. The factor η is the quantum efficiency of the detector, including any dependence on the photosensitive area, which is assumed to be small compared to the coherence area.

We will consider cases where the integrated intensity is separable into a product of modulation-dependent and modulation-independent components

$$W = W_m W_0. \tag{3}$$

This occurs provided the observation interval does not have the same order of magnitude as both τ_m and τ_0.[3–7,13–15] Since W_m and W_0 are statistically independent,

$$P(W) = P(W_m)P(W_0), \tag{4}$$

so that the kth-order moment of W is[15]

$$\langle W^k \rangle = \langle W_m^k \rangle \langle W_0^k \rangle. \tag{5}$$

Using Eqs. (2)–(4) and the well-known Mandel-formula,[18] the probability of emission of n photoelectrons by a plane photocathode illuminated by normally incident, quasimonochromatic, linearly-polarized, intensity-modulated light, is[1–15]

$$p(n,T) = \int_0^\infty \int_0^\infty \left[\frac{(W_m W_0)^n}{n!} \times e^{-W_m W_0} P(W_0)P(W_m)\,dW_0\,dW_m \right]. \tag{6}$$

Employing Eq. (6), the moment generating function of n is

$$\langle e^{tn} \rangle = \int_0^\infty \int_0^\infty e^{W_m W_0 (e^t - 1)} P(W_0)P(W_m)\,dW_0\,dW_m, \tag{7}$$

from which we obtain the kth-order moment of n,

$$\langle n^k \rangle \triangleq \frac{\partial^k}{\partial t^k} \langle e^{tn} \rangle \bigg|_{t=0} = \sum_{j=1}^{k} c_{j,k} \langle W_m^j \rangle \langle W_0^j \rangle, \tag{8}$$

where $c_{1,1} = 1$, $c_{j,k} = 0$ for $j = 0$ or $j > k$, and $c_{j,k} = c_{j-1,k-1} + j c_{j,k-1}$. The kth-order central moment of n can be expressed in terms of the ordinary moments of n as

$$v_k^{(n)} = \sum_{i=0}^{k} \left[(-1)^{k-i} \binom{k}{i} \langle W_m \rangle^{k-i} \langle W_0 \rangle^{k-i} \langle n^i \rangle \right] \tag{9}$$

or in terms of the ordinary and central moments of W as

$$v_k^{(n)} = v_k^{(W)} + \sum_{i=2}^{k} \left[(-1)^{k-i} \binom{k}{i} \langle W_m \rangle^{k-i} \langle W_0 \rangle^{k-i} \times \sum_{j=1}^{i-1} c_{j,i} \langle W_m^j \rangle \langle W_0^j \rangle \right]. \tag{10}$$

In particular,

$$\begin{aligned} v_1^{(n)} &= 0, \\ v_2^{(n)} &= \langle (\Delta n)^2 \rangle = \langle n \rangle + v_2^{(W)}, \\ v_3^{(n)} &= \langle n \rangle + v_3^{(W)} + 3v_2^{(W)}, \\ v_4^{(n)} &= \langle n \rangle + v_4^{(W)} + 7\langle W^2 \rangle + 6\langle W^3 \rangle \\ &\quad + 6\langle W \rangle^3 - 4\langle W \rangle^2 - 12\langle W \rangle \langle W^2 \rangle. \end{aligned} \tag{11}$$

Note that the variance $\langle (\Delta n)^2 \rangle$ is just the sum of the variance of the underlying Poisson distribution and the variance of the modulated intensity. The factorial moments of n are given by

$$\langle n!/(n-k)! \rangle = \langle W_m^k \rangle \langle W_0^k \rangle. \tag{12}$$

Using Eq. (6), we obtain the cumulant generating function of n

$$\ln \langle e^{tn} \rangle = \ln \int_0^\infty \int_0^\infty \left[e^{W_m W_0 (e^t - 1)} \times P(W_0)P(W_m)\,dW_0\,dW_m \right], \tag{13}$$

from which the kth-order cumulant of n is

$$q_k^{(n)} \triangleq \frac{\partial^k}{\partial t^k} \ln \langle e^{tn} \rangle \bigg|_{t=0}, \tag{14}$$

which can be easily evaluated to obtain $q_k^{(n)}$ in terms of $q_k^{(W)}$, $v_k^{(n)}$, or $\langle n^k \rangle$.[19] In particular

$$\begin{aligned} q_1^{(n)} &= \langle n \rangle, \\ q_2^{(n)} &= v_2^{(n)}, \\ q_3^{(n)} &= v_3^{(n)}, \\ q_4^{(n)} &= v_4^{(n)} - 3(v_2^{(n)})^2, \end{aligned} \tag{15}$$

where $v_k^{(n)}$ is given in Eq. (11). The third-order cumulant exhibits the asymmetry of $p(n,T)$.[15] The "broadness" of $p(n,T)$ is indicated by the coefficient of variation $c_v = (q_2^{(n)})^{1/2}/(q_1^{(n)})$. The "length of the tail" of $p(n,T)$ is displayed by the coefficient of skewness $c_s = q_3^{(n)}/(q_2^{(n)})^{3/2}$, whereas the

"peakedness" of $p(n,T)$ is displayed by the kurtosis $c_k = q_4^{(n)}/(q_2^{(n)})^2$. Both c_s and c_k are dimensionless quantities which usually serve as measures of deviation from normality.[20] The skewness and kurtosis of the normal density are $c_s = c_k = 0$, of the uniform density are $c_s = 0$ and $c_k = -1.2$, and of the exponential density are $c_s = 2$ and $c_k = 6$.[20] Under the conditions $T \gg \tau_m$ and $T \gg \tau_0$, $p(n,T)$ is simply Poisson and we find $c_s = \langle n \rangle^{-1/2}$ and $c_k = \langle n \rangle^{-1}$, which approaches the Gaussian result for large n as expected.

ANALYTICAL RESULTS

We use the general results derived above to calculate statistical properties of the photocounting distributions for several radiation sources modulated by various periodic waveforms with uniformly distributed random phase. Since the modulation period T_m is known, it (rather than τ_m) is used to characterize the time scale of fluctuations. Assuming $T \ll T_m$, then $W_m = m(t)$ and $W_0 \int \eta I_0(t')\,dt'$, where the integration is over the observation interval. Although we use periodic modulation waveforms (with random phase) for simplicity of illustration, it is evident from the previous section that our results are applicable to stochastic modulation as well.

The three modulation waveforms considered are the following: (i) Square wave: abrupt transitions between two levels, m_1 and m_2, sustained for equal periods, yielding

$$P(W_m) = (1/2)[\delta(W_m - m_1) + \delta(W_m - m_2)], \quad (16)$$

and

$$\langle W_m^k \rangle = (1/2)\,(m_1^k + m_2^k). \quad (17)$$

(ii) Triangular: linear sweeping between two levels, m_1 and m_2, yielding

$$P(W_m) = (m_2 - m_1)^{-1}, \qquad m_1 \le W_m \le m_2, \quad (18)$$

and

$$\langle W_m^k \rangle = (m_2^{k+1} - m_1^{k+1})/(k+1)(m_2 - m_1). \quad (19)$$

(iii) Sinusoidal: the minimum is m_1 and the maximum is m_2, yielding

$$P(W_m) = \pi^{-1}[(m_2 - W_m)(W_m - m_1)]^{-1/2}, \qquad m_1 \le W_m \le m_2, \quad (20)$$

$$\langle W_m \rangle = (m_1 + m_2)/2,$$

and

$$\langle W_m^k \rangle = \left(2 - \frac{1}{k}\right)\langle W_m \rangle \langle W_m^{k-1} \rangle - m_1 m_2 \left(1 - \frac{1}{k}\right)\langle W_m^{k-2} \rangle, \qquad k \ge 2. \quad (21)$$

The radiation source is assumed to be multimode superposed (interfering) coherent and chaotic radiation (e.g., an amplitude-stabilized laser somewhat above threshold), for which $p(n,T)$ is, to very good approximation, the noncentral negative binomial distribution.[16,21] In this case

$$\langle W_0 \rangle = \langle n_{ch} \rangle + \langle n_c \rangle, \quad (22)$$

and

$$\langle W_0^{k+1} \rangle = \left(\langle W_0 \rangle + \frac{k\langle n_{ch} \rangle}{M}\right)\langle W_0^k \rangle + \frac{\langle n_{ch} \rangle \langle n_c \rangle}{M} \frac{\partial \langle W_0^k \rangle}{\partial \langle n_c \rangle},$$

where $\langle n_{ch} \rangle$ and $\langle n_c \rangle$ represent the mean number of photoelectrons arising from the chaotic and coherent components respectively.[21] The parameter M is the number of modes (M is real, continuous, and ≥ 1); it contains information relative to the spatio-temporal coherence and polarization properties of the light, and the detector integration time and area.[11,16,18,19,21] If $M = \infty$ or $\langle n_{ch} \rangle = 0$, $p(n,T)$ reduces to the Poisson distribution, corresponding to a coherent radiation source (e.g., an ideal amplitude-stabilized laser well above threshold). If $M = 1$ and $\langle n_c \rangle = 0$, $p(n,T)$ reduces to the Bose-Einstein distribution, corresponding to a single-mode chaotic source (e.g., a single-mode laser below threshold, or a narrow spectral line source such as Hg^{198}).

Substituting Eq. (22) and Eq. (17), (19), or (21) into Eq. (8), we obtain the first four ordinary moments of the photocounting distributions for square, sinusoidal, and triangular-wave modulated superposed coherent and chaotic radiation:

$$\langle n \rangle = (1/2)(m_1 + m_2)(\langle n_{ch} \rangle + \langle n_c \rangle),$$
$$\langle n^2 \rangle = \langle n \rangle + f_2 g_2 \langle n \rangle^2,$$
$$\langle n^3 \rangle = \langle n \rangle + 3 f_2 g_2 \langle n \rangle^2 + f_3 g_3 \langle n \rangle^3,$$
$$\langle n^4 \rangle = \langle n \rangle + 7 f_2 g_2 \langle n \rangle^2 + 6 f_3 g_3 \langle n \rangle^3 + f_4 g_4 \langle n \rangle^4, \quad (23)$$

where

$$f_2 = 1 + a\hat{m}^2,$$
$$f_3 = 1 + 3a\hat{m}^2,$$
$$f_4 = 1 + 6a\hat{m}^2 + b\hat{m}^4,$$
$$g_2 = 1 + 2r/M - r^2/M,$$
$$g_3 = 1 + 6r/M - 3r^2/M + 6r^2/M^2 - 4r^3/M^2,$$
$$g_4 = 1 + 12r/M - 6r^2/M + 36r^2/M^2 - 28r^3/M^2 + 24r^3/M^3 - 18r^4/M^3 + 3r^4/M^2,$$

and where $a = b = 1$ for square-wave modulation, $a = 1/2$ and $b = 3/8$ for sinusoidal-wave modulation, and $a = 1/3$ and $b = 1/5$ for triangular-wave modulation. The parameter $\hat{m} \equiv (m_2 - m_1)/(m_2 + m_1)$ is the modulation depth and the parameter $r \equiv \langle n_{ch} \rangle / \langle W_0 \rangle$.

Using Eqs. (23) and (9), we calculate the first four central moments:

$$v_1^{(n)} = 0,$$
$$v_2^{(n)} = \langle n \rangle + (f_2 g_2 - 1)\langle n \rangle^2,$$
$$v_3^{(n)} = \langle n \rangle + 3(f_2 g_2 - 1)\langle n \rangle^2 + (f_3 g_3 - 3 f_2 g_2 + 2)\langle n \rangle^3,$$
$$v_4^{(n)} = \langle n \rangle + 7(f_2 g_2 - 4/7)\langle n \rangle^2 + 6(f_3 g_3 - 2 f_2 g_2 + 1)\langle n \rangle^3 + (f_4 g_4 - 4 f_3 g_3 + 6 f_2 g_2 - 3)\langle n \rangle^4, \quad (24)$$

where f_2, f_3, f_4, g_2, g_3, and g_4 are defined following Eq. (23).

Using Eqs. (23) and (24), we plot as a function $\hat{m}$ the coefficient of variation (Fig. 1), the skewness (Fig. 2), and the kurtosis (Fig. 3) of the photocounting distributions for square (solid curves), sinusoidal (dotted curves), and triangular-wave

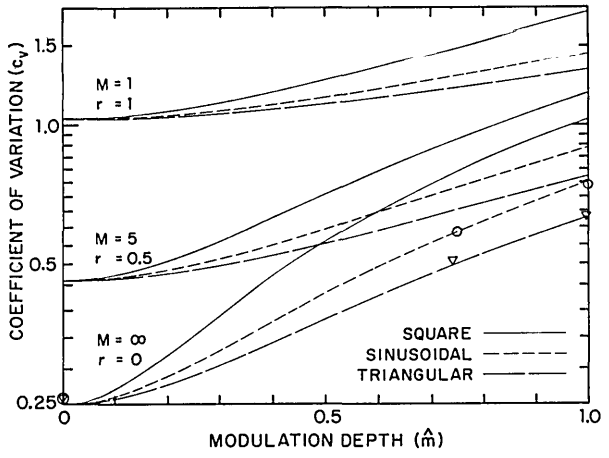

FIG. 1. Plotted as a function of the modulation depth is the logarithm of the theoretical coefficient of variation of the photocounting distributions for square (solid curves), sinusoidal (dotted curves) and triangular-wave (dashed curves) modulated superposed multimode coherent and chaotic radiation with mean count $\langle n \rangle = 16$. The lower set of curves represents the coherent case, for which $r = 0$ and $M = \infty$. The middle set of curves represents the superposed coherent and chaotic case with $r = \frac{1}{2}$ and $M = 5$. The upper set of curves represents the single-mode chaotic case, for which $r = 1$ and $M = 1$. Experimental data points for the triangular (indicated by ∇) and sinusoidal-wave (indicated by O) modulated laser source are shown, for which $T_m = 1$s, $T = 1$ ms, and $N = 10^5$, with exceptions as noted below. In the triangular case, the modulation depth takes on the values $\hat{m} = 0$, $\hat{m} = 0.74$ ($N = 2 \times 10^5$), and $\hat{m} = 0.99$ ($N = 2 \times 10^5$). In the sinusoidal case, the modulation depth takes on the values $\hat{m} = 0$, $\hat{m} = 0.75$ ($T_m = 5$s, $T = 10$ ms, $N = 5 \times 10^4$), and $\hat{m}$ 1 = ($T_m = 5$s, $T = 10$ ms, $N = 5 \times 10^4$).

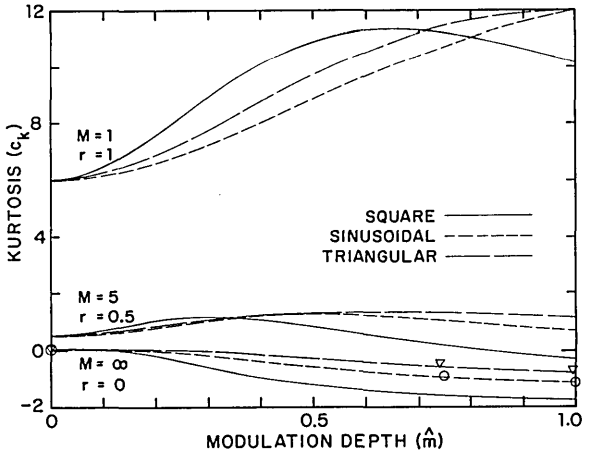

FIG. 3. Kurtosis vs modulation depth. The parameters of all theoretical curves and experimental data shown are identical to Fig. 1.

(dashed curves) modulated superposed coherent and chaotic radiation with $\langle n \rangle = 16$. The lower-most set of curves in Figs. 1–3 represents the coherent case, for which $r = 0$ or $M = \infty$. The middle set of curves in Figs. 1–3 represents the superposed coherent and chaotic case with $r = \frac{1}{2}$ and $M = 5$. The upper-most set of curves in Figs. 1–3 represents the single-mode chaotic case, for which $r = 1$ and $M = 1$.

EXPERIMENT

A series of experiments was performed to verify the statistical properties of the theoretical photocounting distributions computed above for a triangular and sinusoidal-wave modulated laser source. The source was a Spectra-Physics Model 162 Ar^+ ion laser operated at 514.5 nm.[22] The radiation was fed into an acousto-optic modulator that modulated the intensity of the beam with a triangular wave or a sinusoid. The modulated radiation was attenuated sufficiently for the photocounting statistics to be observable and was polarized and detected by an RCA Type 8575 photomultiplier tube. The output pulses from the anode of the photomultiplier tube were registered by a pulse counter.

Data were taken for triangular and sinusoidal-wave modulation for various values of the modulation depth $\hat{m}$. Other experimental parameters were the period of the wave $T_m = 1$ s, the sampling interval $T = 1$ ms, and the number of observation samples $N = 10^5$. These parameters were the same for all sets of data, except where explicitly indicated in the figure captions.

The experimental photocounting data (data points indicated by □, △, ×) as well as the theoretical counting distributions for the same parameters (solid curves) are presented in Figs. 4 and 5 (after Teich and Vannucci, Ref. 13) for trian-

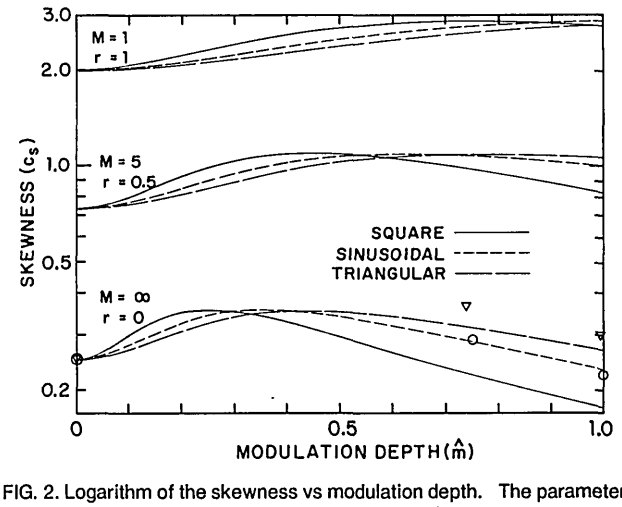

FIG. 2. Logarithm of the skewness vs modulation depth. The parameters of all theoretical curves and experimental data shown are identical to Fig. 1.

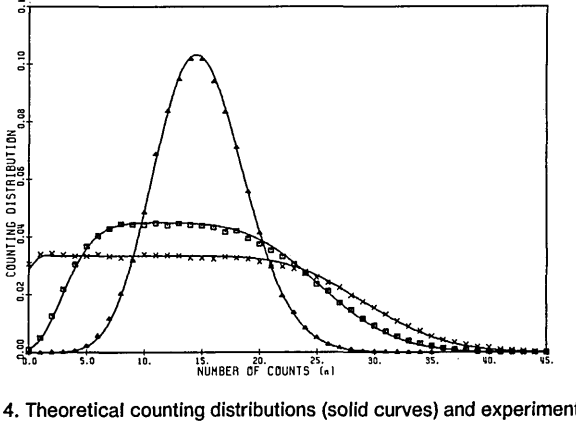

FIG. 4. Theoretical counting distributions (solid curves) and experimental data for triangular-wave modulated coherent radiation. The modulation depth $\hat{m}$ takes on three values: $\hat{m} = 0$ (△), $\hat{m} = 0.74$ (□, $N = 2 \times 10^5$), and $\hat{m} = 0.99$ (× N = 2×10^5). The mean count is approximately the same for all three distributions ($\langle n \rangle = 15$). Note the flat counting distribution [see Refs. 4, 5, and 6] obtained when $\hat{m} \simeq 1$. (After Teich and Vannucci, Ref. 13.)

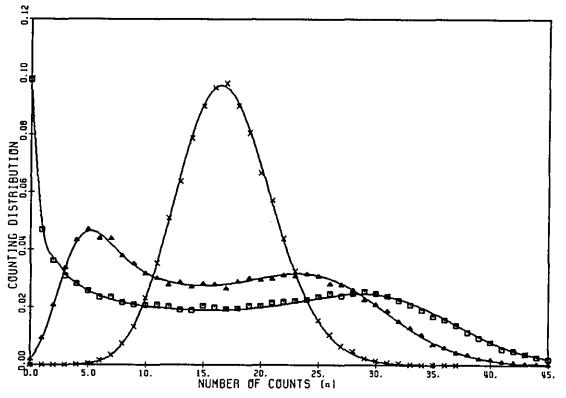

FIG. 5. Theoretical counting distributions (solid curves) and experimental data for sinusoidal-wave modulated coherent radiation. The modulation depth $\hat{m}$ takes on three values: $\hat{m} = 0$ (×), $\hat{m} = 0.75$ (△, $T_m = 5$s, $T = 10$ ms, $N = 5 \times 10^4$), and $\hat{m} = 1.0$ (□, $T_m = 5$s, $T = 10$ ms, $N = 5 \times 10^4$). The mean count is approximately the same for all three distributions ($\langle n \rangle \simeq 17$). (After Teich and Vannucci, Ref. 13.)

gular and sinusoidal-wave modulation respectively [see Eqs. (28) and (37), Ref. 6]. The modulation depth is varied parametrically. The means of the three photocounting distributions for triangular-wave modulation are approximately the same ($\langle n \rangle \simeq 15$), as are the means of the three photocounting distributions for sinusoidal-wave modulation ($\langle n \rangle \simeq 17$).

The experimental coefficient of variation, skewness, and kurtosis (data points indicated by ○, ▽) obtained from each of the above six experimental photocounting distributions, are presented in Figs. 1–3, as a function of $\hat{m}$. The mean corresponding to the theoretical curves in Figs. 1–3 ($\langle n \rangle = 16$) has been chosen to be intermediate between the mean corresponding to the triangular-wave data points (▽, $\langle n \rangle \simeq 15$), and the mean corresponding to the sinusoidal-wave data points (○, $\langle n \rangle \simeq 17$).

DISCUSSION

In examining Figs. 1–3, it is clear that the theory is in good agreement with the experimental data. Where the data does not fall exactly on the theoretical curve, it is primarily because the means of the data and the theoretical curves are slightly different.

We note that the nature of the modulation waveform (i.e., square, sinusoidal, triangular) enters the theoretical equations for the ordinary and central moments [Eqs. (23) and (24)] only through the constants a and b which multiply $\hat{m}^2$ and $\hat{m}^4$ respectively. Also, the parameters $\langle n_{ch} \rangle$ and M appear only as ratios in these equations.

In Fig. 1 we see that increased modulation broadens $p(n,T)$ as expected. Furthermore, c_v is identical for the unmodulated ($\hat{m} = 0$) Bose-Einstein and the fully ($\hat{m} = 1$) square-wave modulated Poisson. As noted earlier, the extent of the broadening (magnitude of c_v) depends strongly on the statistics of the underlying radiation. For example, in Fig. 1 $c_v(\hat{m} = 1)/c_v(\hat{m} = 0)$ is much larger for the Poisson than the Bose-Einstein.

The skewness is positive for all cases in Fig. 2, indicating that $p(n,T)$ is skewed to the right in these cases. However, modulation does not affect c_s [i.e., the length of the tail of $p(n,T)$] in a simple manner, as exhibited by the intersections of the curves. The upper set of curves, representing the Bose-Einstein case, shows that the tail is usually extended by increased modulation. In contrast, the lower set of curves, representing the Poisson case, shows that as $\hat{m}$ approaches unity, the tail decreases in length, reflecting the bimodal shape of $p(n,T)$ [c.f., (△) and (□), Fig. 5, this paper, and Fig. 2, Ref. 6]. The "tapering-off" of c_s in all square-wave cases as $\hat{m}$ approaches unity exhibits the effect of the Dirac-delta component of $p(n,T)$ introduced by full square-wave modulation (see Figs. 1 and 2 of Ref. 6). Furthermore, c_s is relatively constant for the triangular-wave modulated Poisson case, since in this case (see Fig. 4) when $\hat{m} = 0$, $p(n,T)$ is nearly Gaussian in shape (for which $c_s = 0$), and when $\hat{m} = 1$, $p(n,T)$ is nearly uniform in shape (for which c_s also = 0).

The kurtosis of the modulated Poisson is usually negative in Fig. 3, indicating that $p(n,T)$ is flattened by modulation. Whereas $c_k = -1.2$ for the uniform density, $c_k \simeq -0.7$ for the fully triangular-wave modulated Poisson, which exhibits extreme flatness (see Fig. 4, this paper, and Refs. 4 and 5). In contrast, c_k for the modulated Bose-Einstein is positive, and generally increases with $\hat{m}$, indicating that modulation causes $p(n,T)$ to become more sharply peaked (see Figs. 1 and 4 of Ref. 6). We note that $c_k = 6$ for both the unmodulated Bose-Einstein and the exponential distribution, emphasizing their similarity in shape.

ACKNOWLEDGMENT

This work was supported by the National Science Foundation with supplemental support from the Joint Services Electronics Program.

[1]G. J. Troup, "A technique for determining the photoelectric counting distributions for some ideal systems," IEEE J. Quantum Electron. **QE-1**, 398 (1965).
[2]S. Fray, F. A. Johnson, R. Jones, T. P. McLean, and E. R. Pike, "Photon-counting distributions of modulated laser beams," Phys. Rev. **153**, 357–359 (1967).
[3]P. Pearl and G. J. Troup, "Modulated laser beam photon counting distributions," Phys. Lett. **27A**, 560–561 (1968). Equation (3) in this paper is incorrect and should be replaced by Eq. (38) of Ref. 6.
[4]M. C. Teich and P. Diament, "Flat counting distribution for triangularly-modulated Poisson process," Phys. Lett. **30A**, 93–94 (1969).
[5]M. C. Teich and P. Diament, "Observation of flat counting distribution for Poisson process with linearly-swept mean," J. Appl. Phys. **41**, 415–416 (1970).
[6]P. Diament and M. C. Teich, "Photoelectron-counting distributions for irradiance-modulated radiation," J. Opt. Soc. Am. **60**, 682–689 (1970).
[7]P. Diament and M. C. Teich, "Photodetection of low-level radiation through the turbulent atmosphere," J. Opt. Soc. Am. **60**, 1489–1494 (1970).
[8]C. Bendjaballah and F. Perrot, "Distributions de photoélectrons d'une lumière laser modulée sinusoïdalement," C. R. Acad. Sci. (Paris) **271**, 1085–1088 (1970).
[9]M. C. Teich and S. Rosenberg, "N-fold joint photocounting distribution for modulated laser radiation: Transmission through the turbulent atmosphere," J. Opto-electron. **3**, 63–76 (1971).
[10]W. G. Clark and E. L. O'Neill, "Photoelectron count distributions due to periodic irradiance modulation," J. Opt. Soc. Am. **61**, 934–938 (1971).
[11]L. Mišta, "Counting distribution for M-mode superposition of chaotic and modulated coherent fields," Czech. J. Phys. **B23**, 715–718 (1973).
[12]I. Kitazima, "Photon-counting distribution under square-wave

intensity modulation," Opt. Commun. 10, 137–140 (1974).
[13]M. C. Teich and G. Vannucci, "Observation of dead-time-modified photocounting distributions for modulated laser radiation," J. Opt. Soc. Am. 68, 1338–1342 (1978).
[14]M. C. Teich and H. C. Card, "Photocounting distributions for exponentially decaying sources," Opt. Lett. 4, May (1979).
[15]B. Saleh, *Photoelectron Statistics* (Springer-Verlag, New York, 1978).
[16]M. C. Teich and W. J. McGill, "Neural counting and photon counting in the presence of dead time," Phys. Rev. Lett. 36, 754–758, 1473 (1976).
[17]G. Vannucci and M. C. Teich, "Effects of rate variation on the counting statistics of dead-time-modified Poisson processes," Opt. Commun. 25, 267–272 (1978).
[18]L. Mandel, "Fluctuations of photon beams: The distribution of the photo-electrons," Proc. Phys. Soc. 74, 233–243 (1959).
[19]J. Peřina, *Coherence of Light* (Van Nostrand Reinhold, New York, 1971), p. 128.
[20]M. Woodroofe, *Probability with Applications* (McGraw-Hill, New York, 1975), p. 238.
[21]J. Peřina, "Superposition of coherent and incoherent fields," Phys. Letters 24A, 333–334 (1967); "Superposition of thermal and coherent fields," Acta Universitatis Palackianae Olomucensis Facultas Rerum Naturalium 27, 227–234 (1968).
[22]Though this laser oscillates on a number of longitudinal modes, the photocounting statistics are effectively the same as those of an amplitude-stabilized source under the conditions of our experiment. See Ref. 13 and T. Aoki, Y. Endo, and K. Sakurai, "Photon statistics and autocorrelation of a multi-mode laser," Opt. Commun. 23, 26–28 (1977).

Statistics of the optical transfer function: Correlated random amplitude and random phase effects

Elliot Blackman
Bolt Beranek and Newman Inc., Cambridge, Massachusetts 02138

Richard Barakat
Division of Applied Sciences, Harvard University, Cambridge, Massachusetts 02138
Bolt Beranek and Newman Inc., Cambridge, Massachusetts 02138

(Received 31 August 1978)

The pupil function of an optical system is taken to have correlated random amplitudes and phases arising from an external cause, such as optical propagation through turbulence. For the general case, where the restriction of isotropy need not apply, the unnormalized random optical transfer function is derived and its first two moments evaluated. Normalization issues are also treated. It is shown that when the cross correlation of random amplitude and random phase is not an even function, a phase shift term is induced. The impact of this shift is discussed in terms of the image of an edge. While isotropy eliminates dependence on the cross correlation of amplitude and phase for the first moment of the transfer function, it does not similarly affect all second-moment behavior.

INTRODUCTION

The influence of random wave front and random amplitude on the optical transfer function is a continuing problem in optical imagery. The mean value of the optical transfer function has been evaluated by several investigators[1–5] for a variety of conditions. The second moments and Monte Carlo simulations have been considered in[6] for the random wavefront case.

The purpose of the present paper is to study the behavior of the optical transfer function, through its first two moments, when the random wave front and random amplitude of the pupil function are correlated. It is shown that the effect of the cross correlation of amplitude and phase is to include a phase-shift term in the transfer function.

In order to simplify typography, we limit ourselves to the one-dimensional (slit aperture) situation. The extension to two dimensions is purely formal.

FIRST MOMENT

The unnormalized transfer function $R(\alpha)$ for a slit aperture is equal to the convolution of the pupil function $A(p)$

$$R(\alpha) = \int_{-b}^{b} A\left(p + \frac{1}{2}\alpha\right) A^*\left(p - \frac{1}{2}\alpha\right) dp, \tag{1}$$

where $b \equiv (1 - |\alpha|/2)$ and $|\alpha| \leq 2$. The pupil function is given by

$$A(p) = A_0(p) \exp[ikW(p)], \tag{2}$$

where $A_0(p)$ and $W(p)$ are real.

$W(p)$ is the aberration function (Hamilton's mixed characteristic function), and is taken to consist of the sum of a deterministic term due to the intrinsic aberrations of the optical system $W_D(p)$ and a term due to the random atmosphere $Z(p)$; thus $W(p) = W_D(p) + Z(p)$. $Z(p)$ is taken to be a zero mean, spatially stationary, real Gaussian random process

$$E[Z(p)] = 0, \tag{3}$$

$$E[Z(p_1)Z(p_2)] = \sigma_z^2 r_z(p_1 - p_2), \tag{4}$$

where r_z is the correlation function and σ_z^2 is the variance.

Without actually specifying the probability density function (PDF) of $A_0(p)$, we take the mean of $A_0(p)$ to be given by

$$m_A \equiv E[A_0(p)] = A_0(\approx 0.6\text{–}0.8). \tag{5}$$

Furthermore, $A_0(p)$ is taken to have a small variance σ_A^2 so that the PDF of $A_0(p)$ is peaked around A_0. Given these considerations, we set $A_0(p) = \exp[\psi(p)]$, where $\psi(p)$ is a real, stationary, Gaussian random process [i.e., $A_0(p)$ is lognormally distributed]. Consequently,

$$E[\psi(p_1)\psi(p_2)] = \sigma_\psi^2 r_\psi(p_1 - p_2). \tag{6}$$

 0030-3941/79/040544-05$00.50